SYNTHESIS AND CHARACTERIZATION OF CHALCOGEN BASED MATERIALS IN GLASSY AND NANOSTRUCTURED FORMS: A REVIEW

*Gurinder Kaur[1] and M.S. Bakshi[2]
[1]*Materials and Nanotechnology Research Laboratory,*
College of the North Atlantic
1600 Nichols Adam Highway
Labrador City, NL A2V 0B8, Canada
*(*Corresponding author: gurinder.kaur@cna.nl.ca)*

[2]*Department of Chemistry*
Wilfred Laurier University, Science Building
75 University Ave. W., Waterloo ON N2L 3C5 Canada.

SYNTHESIS AND CHARACTERIZATION OF CHALCOGEN BASED MATERIALS IN GLASSY AND NANOSTRUCTURED FORMS: A REVIEW

ABSTRACT

Selenium (Se) based materials find wide applications in rectifiers, solar cells, photographic exposure meters, data storage devices, xerography and anticancer agents. They are also used in the glass industry to eliminate bubbles and remove undesirable tints produced by iron. In addition, Se is highly reactive towards a wealth of chemicals that can be potentially exploited to convert Se into other functional materials such as CdSe, ZnSe, Ag_2Se. Here, we report a review of structural investigations of Se based materials in glassy and nanostructured forms. Glasses having varying amounts of Se and Tellurium (Te) were doped with group IV and V elements such as antimony and tin. Structural changes accompanying the composition variation were characterized with x-ray photoelectron spectroscopy, differential scanning calorimetry and x-ray absorption near edge spectroscopy. At the same time Se-Te nanoalloys were synthesized in aqueous micellar phase using Na_2SeO_3/Na_2TeO_3 as the Se/Te source. Morphology change from nanoparticles to nanoribbons was investigated using Scanning and Transmission Electron Microscopy (SEM/TEM) techniques. Structural investigations were also done for well defined morphologies of Se based nano-biomaterials obtained in the presence of water soluble protein bovine serum albumin (BSA).

INTRODUCTION

Components of next generation technologies such as semiconductor nanocrystals are going to be materials with nanometric dimensions with many useful applications in lasers, photovoltaics, light emitting diodes and biological assays. Chalcogen (Group VI elements- selenium (Se), tellurium (Te), sulphur (S)) based semiconducting materials are promising candidates for a wide variety of applications such as data storage devices, solar cells, biological imaging, infrared photo detectors and communication devices. The ability to tune the electrical and optical properties of semiconductor nanocrystals by manipulating the size and shape of the crystals during the colloidal synthesis provides potential benefits to a variety of applications including photovoltaic devices, light emitting diodes, field effect transistors, biological imaging/labeling and more. Both (Se) and (Te) exist in helical chains (Figure 1) in crystalline form. Se exhibits photovoltaic action by converting light into electricity through photoconductivity due to its reasonably small band gap of 2.6 eV in crystalline form. This allows Se to be used in versatile photocells and solar cells as reported by Zingaro et al. (1974) and Berger (1997). Te also exhibits photoconductivity to a lesser extent. Both Se and Te are p-type semiconductors and hence used in electronics and solid-state application. Some of the properties and effects which make these materials suitable for various applications are shown in Figure 2. Independently, both predominantly form 1D nanostructures (Lu et al., 2005; Gates et al., 2000) due to a preferential growth along the c-axis of trigonal hexagonal geometry as a result of their unique tendency to exist in the spiral chains. 1D geometries have potential ramifications in electronic device formation (Hu et al., 2000). Facile production of such morphologies under economical favourable conditions such as in aqueous phase and at relatively low temperature (< 100 ^{o}C) is always required. Recently, Se – Te alloys have been found to demonstrate interesting temperature dependence of electrical resistivity (Baitser & Vainberg, 1996).

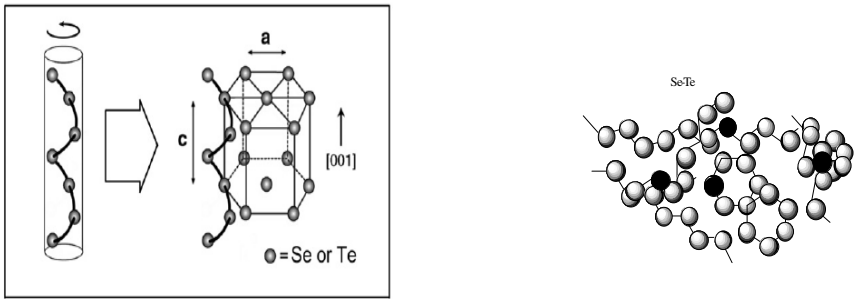

Figure 1 – Structure of crystalline Se-Te

In addition, fine homogenous nearly monodisperse Se – Te nanorods have also been synthesized simply by following hydrazine reduction. The aim of this work is to review synthesis and characterization of some of the Se based materials in view of their practical applications carried out in our work over the last several years. The investigations include synthesis of glasses having compositions Se-Te-X (X= Sb, Pb, Sn, In) and characterization of their structure, electrical and optical properties. This was followed by nanostructuring of materials having similar compositions using colloidal chemical synthesis techniques.

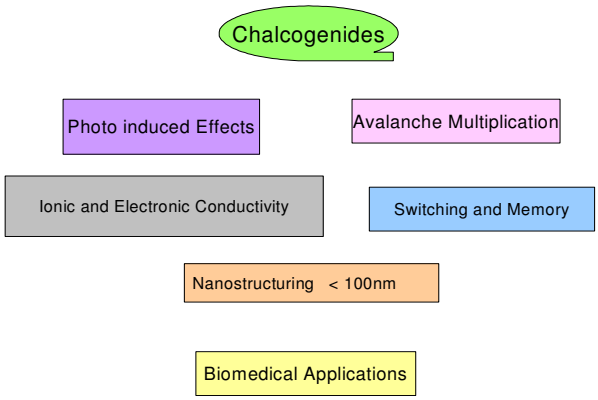

Figure 2 – Important properties and effects observed in chalcogenide glasses which make them suitable for various applications

RESULTS AND DISCUSSIONS

Non-Linear Optical Properties

Materials exhibiting non-linear optical properties are attractive candidates for future high bit rate optical communication .Silica based optical fibers are one of the most promising media for such all-optical switches (Meyers et al., 2001, Morioka & Saruwatari 1998). However, these switches demand relatively high switching power or fiber lengths because of the small non-linear refractive index ($n_2 \sim 2.8 \times 10^{-16}$ cm^2/W) of silica glasses. In an effort to solve this problem, other glasses with large non-linearities are being studied (Nelsen et al., 1991; Newhouse et al., 1990). Chalcogenide glasses are promising candidates for these applications due to their high optical nonlinearity. Several chalcogenide compositions have been shown to exhibit large values of non-linear refractive index, n_2, together with low absorption in the 1–1.5 micrometers telecommunications window (Petkov & Even, 1999). For As–S–Se glasses investigated by Asobe et al. (Cerqua Richardson et al., 1998) values of n_2 up to 400 times that of silica have been reported. Such large values have been correlated with the presence of covalent, homopolar Se–Se bonds in the glass. It is possible that compositions with even stronger non-linearity may exist and a method for predicting such

compositions would be useful. It is widely known that second order non-linear susceptibility can exist only in the non-centrosymmetric materials. Therefore, SHG in a homogeneous glass is forbidden due to spherical symmetry of the glass. In particular, SHG can initiate as a result of the presence of nano-sized inhomogeneities both crystalline and amorphous leading to non-linear light scattering. Se (symmetry 32) and Te (symmetry32) have been known to possess phase matching properties and exhibit large second order non-linearities (Cardinal et al., 1999). However, the low values of the thermal parameters (such as glass transition temperature) and the limitations imposed by the mechanical properties of these materials in elemental form necessitate their alloying with other group III or group V elements for practical applications.

Glass Synthesis

Bulk amorphous Se_{80-x}–Te_{20}–Sb_x ($0<x<9$ at. %) materials were synthesized by the conventional melt quenching technique. Appropriate amounts of 5N purity elements Se, Te, Sb were sealed in quartz ampoules at a pressure of ~10^{-5} Torr. The ampoules were kept in a rocking furnace at a temperature of 650 °C for 48 h under controlled heating conditions. The ampoules were quenched in ice water, and the bulk glass was retrieved from the ampoule by dissolving it in a mixture of hydrogen peroxide and hydrofluoric acid for 48–72 h.

Surface Second Harmonic Generation in $Se_{80-x}Sb_xTe_{20}$ ($0<x<9$)

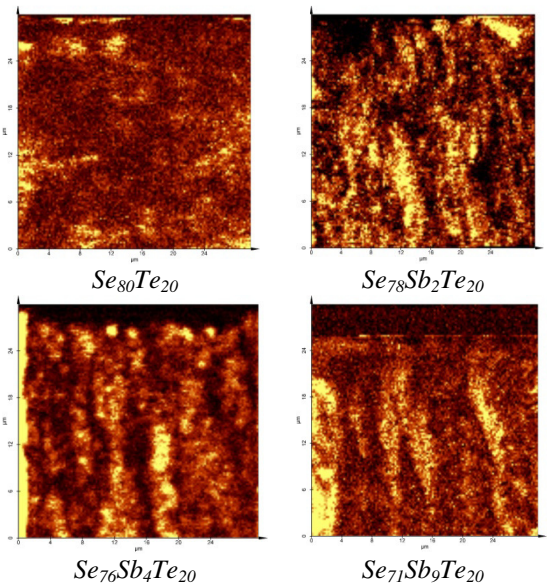

Figure 3 – SSHG images of $Se_{80-x}Sb_xTe_{20}$ ($0 < x < 9$ at. %) films obtained at 393 nm by the confocal scanning microscope

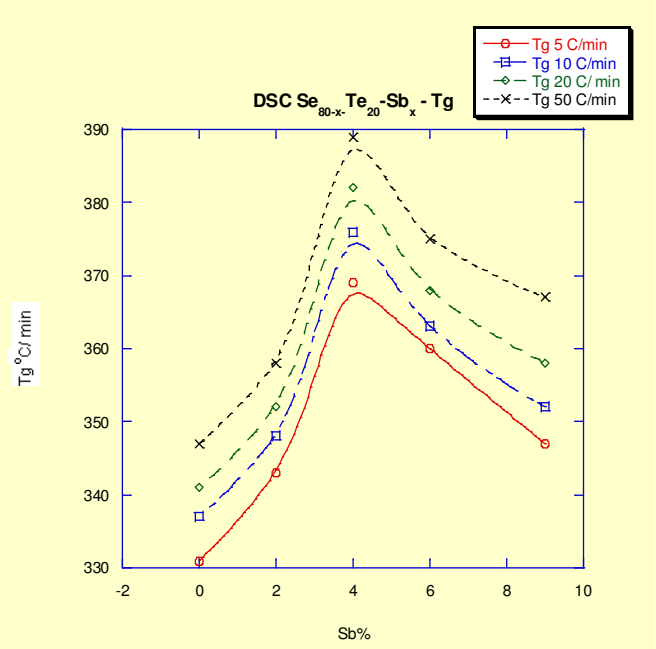

Figure 4 – Variation of the glass transition temperature from differential scanning calorimetry

Surface second harmonic generation in thin films of amorphous Se–Te doped with antimony (Sb) are shown in Figure 3. Results have been investigated on the basis of interplay of experiment and theory in connection with the local electronic structure and corresponding changes in the band structure of the material. A remarkable change in the behavior of the SHG intensity caused by changing Se:Sb ratio keeping the tellurium content constant at 20 at.% in the $Se_{80-x}Sb_xTe_{20}$ ($0 < x < 9$) system can be seen in Figure 4. A marked difference in the magnitude of the signal generated by the samples with an antimony content < 4 at.% and those containing antimony > 4 at.% can explained on the basis of charge distribution associated with structural changes in these materials for different compositions (Mehra et al., 1991). This has been ascribed to a variety of relatively isolated atomic events that occur at short length scales mainly on the basis of spatial redistribution of covalent bonds, the rational changes in the electric dipole moment arising from the lone pair electron orbitals constituting the valence band, inherent in chalcogenide glasses. These results are supported by the variation of the glass transition temperature obtained from differential scanning calorimetry. Structural changes caused by the compositional variation leads to changes in the electron density.

Theoretical Considerations

In order to explain the observed behavior of the second harmonic generation signal of the samples, we investigated the electronic configurations of the ground states of the Se, Se_3Te and Se_2TeSb systems theoretically. The ground states of the Se systems were evaluated using self-consistent DFT through the WIEN code (Blaha et al., 1990).

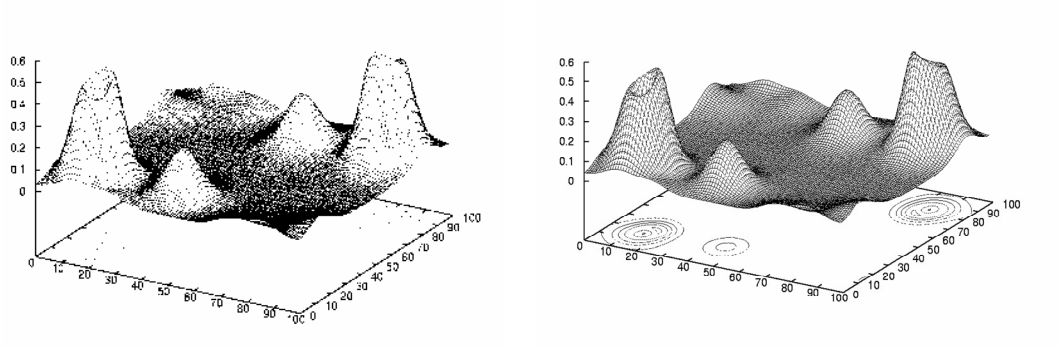

Figure 5 – Density functional theory plots for pure Se, Se_3Te and Se_2SbTe

The Kohn Sham equation was solved self-consistently by the full potential linearized augmented plane wave method. The unit cell of the considered sample has been divided into two regions: (1) the non-overlapping atomic spheres and (2) an interstitial region .Inside the atomic sphere, a linear combination of radial functions times the spherical harmonics Y_{lm} (r) is used .In the interstitial region a plane wave expansion is utilized spheres. The boundary condition is met where the basis functions and their derivatives are matched at the atomic spheres. The Generalized Gradient Approximation was added to the DFT calculation with 1,000 points. The bulk Se system is chosen to be the alpha- monoclinic structure with four symmetric positions. The values of the lattice constants and angles of the unit cell used for calculations are a = 9.054 pm, b = 9.083 pm, c = 11.601 pm, and beta= 90.81°. The Se_3Te system as shown is constructed by substituting Te atom to one of the four Se symmetric sites of the Se crystals. The Se_2TeSb system is calculated by substituting each of the Te and Sb atoms into one of the four Se symmetric sites. Figure 5 shows the electron distributions along the [100] plane of the Se, Se_3Te, and Se_2TeSb systems. It can be seen that the electrons move further away from the nucleus as the Se atomic sites in the crystal are replaced with Te and Sb atoms. The structure of Se–Te can thus be considered to consist of a mixture of Se–Te rings and long chains extending up to a short range order permissible in the amorphous structure. Addition of Sb causes a lengthening of the chains due to cross-linking. For samples containing Sb < 4 at.% the non-linear susceptibility increases as the Sb content increases due to a higher displacement of the electronic cloud extending in the structure along the length of the chains. This leads to a higher electric dipole moment associated with the structure and a corresponding higher non-linear susceptibility with a corresponding increase in the SSHG signal. This is supported by the observations of the SSHG pattern observed for samples containing Sb < 4 at. %. Since Se is more electronegative as compared to Sb, these observations indicate the aggregation of Sb along Se–Te chain.

Structure

We used x-ray photoelectron spectroscopy (XPS) and x-ray absorption near edge spectroscopy (XANES) at the Se site, probing the occupied and unoccupied (Se character) electronic states below and above the Fermi levels, respectively. The changes in the electronic structure caused by changing the Se: Sb ratio while keeping the tellurium content constant at 20 at. % in the $Se_{80-x}Sb_xTe_{20}$ ($0<x<9$) alloy have been investigated. The XPS of the valence band (VB) spectra of the $Se_{80-x}Te_{20}Sb_x$ systems with x=2, 4, and 9 are shown in Fig. 6. The measurement tracks the occupied DOS convoluted by experimental resolution and X-ray photoelectron cross section (Chung et al., 2004). The VB is dominated by Se and, to a lesser extent, by Te contributions as indicated by the composition. The theoretically calculated DOS of the Se_2TeSb crystal using method 1 have been plotted together with the XPS VB of the Se–Te–Sb systems for comparison. It can be seen that as the Sb content increases from 2–9 at. %, the VB of the $Se_{80-x}Te_{20}Sb_x$ systems narrows, and the top of the band as well as the centroid of the band moves toward the Fermi level. This reduction in VB bandwidth (*sp* band narrowing) can be interpreted as a dilution effect such that the presence of Sb has disrupted the strong Se–Se and Se–Te interaction, which dominates the bandwidth. It is generally recognized that the bandwidth of noble metals and metalloids is proportional to the number of

"like" nearest neighboring atoms, in this case, Se and Te. If Sb plays the role of dilution, disrupting the Se–Se and Se–Te interaction by substitution, then the band will become narrow .The movement of the VB and the narrowing of bandwidth upon alloying have been observed in noble metals and have been well understood (Assoud et al., 2004). Close examination reveals that while change is clearly noticeable going from x=2 to x=4, the VB changes very little from x=4 to x=9, indicating that the effect of Sb dilution may reach saturation at x=4.

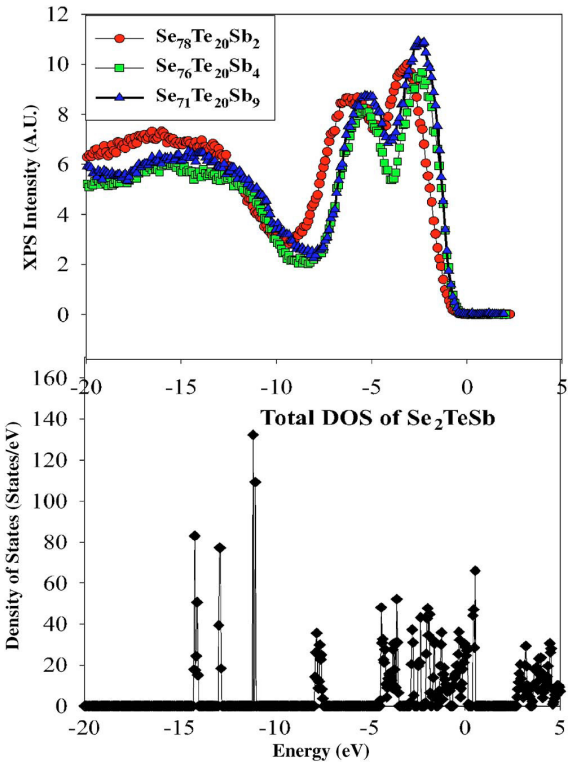

Figure 6 – Valence band structure of the Se-Te-Sb alloys

Nanostructured Materials: **Nano-Selenium**

Bio-nanomaterials are highly important constituents of biocompatible devices with many applications in bioengineering, biomedical imaging, molecular diagnostics, and most importantly a new class of hybrid materials. Material properties affect biological outcomes including the half-life of drugs, biocompatibility of implanted devices, and release rates and toxicity of drug carriers. Similarly, physical and chemical properties of biomaterials can have a profound impact on cell proliferation and remodeling of tissues. A precise shape-controlled synthesis of a biomaterial is possible only if capping biomolecules could selectively control the crystal growth.

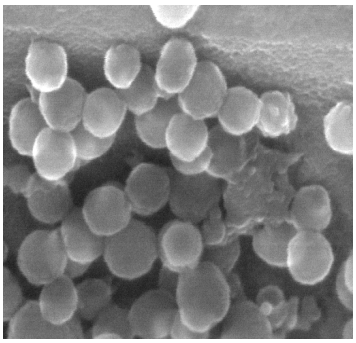

Figure 7 – BSA capped Se nanoparticles

More recently, bovine serum albumen (BSA), a water-soluble and highly important carrier protein, showed remarkable shape-controlled effects on PbS nanocrystals with respect to a temperature variation within 40–80 °C. The unfolded form of BSA worked effectively in controlling the crystal structure and led to well-defined cubic nanomorphologies in comparison to its native folded state. The exposed hydrophobic domains of unfolded form provided desired surface activity to control the crystal growth .Use of a carrier protein like BSA in a shape-controlled synthesis of bio-nanomaterials provides a direct opportunity to produce desired biomaterials for devices with applications in bioengineering. Se particles were synthesized by a chemical reduction of sodium selenite by hydrazine. In a typical procedure, 10 mL of aqueous BSA ($1–10 \times 10^{-4}$ g/mL) along with 2.5% hydrazine was taken in a round bottom glass flask. Under constant stirring, sodium selenite (6–25 mM) was added in it and kept at 85 °C for 48 h. The color of the solution changed from colorless to deep orange within 2 h and remained same till 48 h. Initial pH of BSA + water solution was 6.7 which increased to 7.8 upon addition of hydrazine. Addition of Na_2SeO_3 further increases the pH = 9 due to the following reaction

$$N_2H_4\,(aq) + SeO_3^{2-}\,(aq) \rightarrow Se\,(s) + N_2\,(g) + 2OH^-\,(aq) + H_2O \qquad (1)$$

Within 2 h, pH further rises to 11 due to the denaturation of BSA (at 85 °C) and remained fairly constant for 48 h. The samples were purified by spinning the reaction product at 10,000 rpm for 10 min. with repeated washing from distilled water. Pictures of Se nanoparticles taken using SEM are shown in Figure 7.

Results conclude that BSA works well in controlling the overall geometry of nanoparticles when [Na_2SeO_3/BSA] mole ratio is ≈ 6. At this mole ratio, denatured BSA becomes even more hydrophobic due to the neutralization of oppositely charged sites by SeO_3^- ions. A predominantly hydrophobic BSA is a better shape directing agent. But at too high mole ratio = 28, BSA proves to be a poor capping agent due to the presence of too many nucleating centres whose growth cannot be simultaneously controlled by BSA macromolecules. On the other hand, when the mole ratio ≈ 1, then unfolded BSA macromolecule works as a soft template by accommodating maximum nucleating centres on it and thereby facilitating the Ostwald ripening. Therefore, in order to have a best shape directing effect of BSA, following features must be taken in care. (a) BSA should be in unfolded and predominantly hydrophobic state. (b) The precursor concentration should be greater than that of BSA so that growing nucleating centres can be properly stabilized. (c) Too many nucleating centres cannot be simultaneously stabilized by BSA due to its time dependent surface adsorption

.

Se – Te Nano-Alloys: Morphology Control from Nanoparticles to Nanoribbons with Non-ideal mixing

Se – Te NCs were synthesized by a simultaneous hydrazine reduction of both aqueous Na_2SeO_3 and Na_2TeO_3 in a micellar solution. First of all, two aqueous stock solutions of Na_2SeO_3 = 25 mM and Na_2TeO_3 = 25 mM were prepared separately in the presence of CTAB = 50 mM. Required quantities of both stock solutions were mixed to produce different Se mole fractions, X_{Se} = 0, 0.2, 0.4, 0.6, 0.8, and 1, with total (Na_2SeO_3 + Na_2TeO_3) = 25 mM, along with a constant addition of 3.6 M hydrazine in each case.

The reaction bottles with final volume of 10 mL of each mole fraction were then kept in an oil bath maintained at 85 °C for 24 h under static conditions. Similar set of reactions were also carried out in the presence of 0.1 M and 2.2 M hydrazine while keeping the concentrations of all other ingredients constant. The color of the solution changed from colorless to brown – black for the mole fractions lying in the Se rich-region, while colorless to grey – black for those lying in the Te rich-region of the mixtures within 2–4 h and remained the same until 48 h. The colloidal suspensions thus obtained were cooled to room temperature. NCs were collected after repeated washing with pure water (at least 3 times) to remove excess of surfactant followed by spinning at 10,000 rpm for 5 min in each case. Pictures of nanoparticles obtained using TEM are shown in Figure 8.

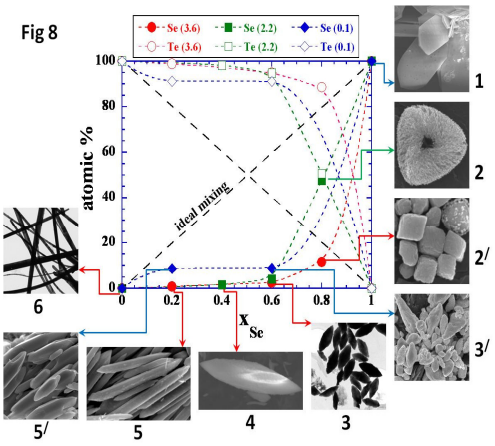

Figure 8 – A plot of atomic % of Se and Te in Se – Te alloy NCs versus stochiometric mole fraction of Se (x_{Se}) over the whole composition range of Se + Te mixtures in the presence of 3.6 M (red symbols), 2.2 M (green symbols), and 0.1 M (blue symbols) hydrazine .Empty and filled symbols belong to Te and Se atomic %, respectively

The results conclude that fine crystalline Se – Te alloy morphologies can be obtained over the whole composition range of Se and Te mixtures. But the shape, structure, and elemental composition of different morphologies depend very much on the amount of reducing agent (i.e. hydrazine). Three concentrations of hydrazine viz. 3.6 M, 2.2 M, and 0.1 M have been used to determine the influence of reducing agent on the overall morphology at a particular mole fraction. The concentrations 3.6 M and 2.2 M are considered to be in excess in comparison to 0.1 M of hydrazine, as well as in comparison to 25 mM of Se and Te sources. Excess of hydrazine produces amorphous water soluble Se nanoparticles and fine crystalline Te nanoribbons of several micrometers in length. Their different mixing ratios on the other hand produce different morphologies with regular transitions from rhombohedral NCs in the Se rich-region to spindle shaped NCs close to equimolar proportions, and then to fine crystalline needles in the Te rich-region of the mixtures. All morphologies show a complete homogenous mixing between elemental Se and Te in Se – Te alloy but with a marked non-ideal behaviour with respect to their stochiometric mole fractions over the total mixing range. All morphologies show a significantly low Se and high Te contents than their ideal amounts. The degree of non-ideality decreases in the order of 3.6 M > 2.2 M > 0.1 M of hydrazine, which means excess of hydrazine produces crystalline Se – Te alloys with significantly higher amounts in elemental Te. These findings have been attributed primarily to the non-metallic nature of Se and metalloid nature of Te. A reduction of SeO_3^{-2} ions by excess of hydrazine produces many nucleating centres with amorphous nature which have predominantly greater affinity for aqueous phase. In contrast, TeO_3^{-2} ions produce crystalline nucleating centres with greater probability of existing heterogeneously in aqueous phase. Thus, in the mixed state Se – Te alloy NCs possess greater amount of Te even in the Se rich-region of the mixtures. However, as the amount of hydrazine is reduced to 0.1 M, relatively fewer number of Se nucleating centres are produced and they undergo autocatalytic process with other SeO_3^{-2} ions to ultimately produce large flake like morphologies. A low hydrazine concentration also influences

the shape, structure, and composition of different morphologies predominantly lying in the Se rich-region but with little effect on the morphologies of Te rich-region. Thus, this study provides an easy access to facile synthesis of different morphologies of Se – Te alloy NCs simply by varying the amount of hydrazine. One dimensional Se – Te alloy nanoribbons and long needles can find their way to low cost versatility and large scale production for their industrial applications in optoelectronic and device formation.

ACKNOWLEDGMENTS

The authors extend sincere thanks to funding agencies RDC, Newfoundland and Labrador, and NSERC, Canada for supporting the work .We also thank our collaborators from University of Western Ontario for their contributions to the original work presented as a review in this work.

REFERENCES

Assoud, A., Derakhshan, S., Soheilnia, N., Kleinke, H. (2004). Chemistry of Materials, 16, 4193.

Baitser, R. I., Vainberg, V. V. Varshava, S. S., (1996). Journal of Physics IV 6, C3–429.

Berger, L.I., (1997). Semiconductor Materials; CRC Press: Boca Raton, FL, p86.

Blaha, P., Schwarz, K., Sorantin, P., Trickey, S.B., (1990). Computational Physics Communications, 59, 399.

Cardinal, T., Richardson, K.A., Shim, H., Schulte, A., Beatty, R., Foulgoc, K. Le, Meneghini, C., Viens, J.F., Cerqua-Richardson, K.A., McKinley, J.M., Lawrence, B., Joshi, S., Villeneuve, A., (1998). Optics Materials 10, 155.

Chung, D. Y. Hogan, T. P., Rocci-Lane, M. Brazis, P. Ireland, J. R.; Kannewurf, C. R. Bastea, M. Uher C., Kanatzidis, M. G., (2004). Journal of American Chemical Society 126, 6414.

Gates, B. Yin, Y. Xia, Y., (2000). Journal of American Chemical Society, 122, 12582.

Hu, J., Odom, T. W., Lieber, C. M., (1999). Accounts of Chemical Research 32, 435.

Lu, Q., Gao, F., Komarneni, S., (2005). Chemistry of Materials, 18, 159.

Mayers, B., Byron, G., Yin, Y., Xia, Y., (2001). Advanced Materials, 13, 1380.

Mehra, R. M., Kaur, G., Mathur ,P.C., (1991). Journal of Materials Science, 26, 3433-3437.

Morioka, T., Saruwatari, M., (1988). IEEE J. Selected Area Communications 6, 1186.

Nelson, B.P., Blow, K.J., Constantine, P.D., Noran, N.J., Lucek, J.K., Marshall, I.W., Smith, K., (1991). Electronics Letters 27, 704.

Newhouse, M.A., Weidman, D.L., Hall, D.W., (1990). Optics Letters, 15, 1185.

Petkov, K., Ewen, P.J.S., (1999). Journal of Non-Crystalline Solids, 249, 150–159.

Villeneuve, A., (1999). Journal of Non- Crystalline Solids, 256, 257, 353.

Zingaro, R.A., Cooper, W.C., (1974). Eds.: Selenium, Lutton Educational Publishing: New York, Pp 25 and 174-217.